Acoustic anechoic layers with singly periodic array of scatterers: Computational methods, absorption mechanisms, and optimal design*

Yang Hai-Bin(杨海滨), Li Yue(李 岳), Zhao Hong-Gang(赵宏刚), Wen Ji-Hong(温激鸿), and Wen Xi-Sen(温熙森)†

Vibration and Acoustics Research Group, Laboratory of Science and Technology on Integrated Logistics Support, College of Mechatronics and Automation, National University of Defense Technology, Changsha 410073, *China*

(Received 30 December 2013; revised manuscript received 7 March 2014; published online 20 August 2014)

The acoustic properties of anechoic layers with a singly periodic array of cylindrical scatterers are investigated. A method combined plane wave expansion and finite element analysis is extended for out-of-plane incidence. The reflection characteristics of the anechoic layers with cavities and locally resonant scatterers are discussed. The backing is a steel plate followed by an air half space. Under this approximate zero transmission backing condition, the reflection reduction is induced by the absorption enhancement. The absorption mechanism is explained by the scattering/absorption cross section of the isolated scatterer. Three types of resonant modes which can induce efficient absorption are revealed. Due to the fact that the frequencies of the resonant modes are related to the size of the scatterers, anechoic layers with scatterers of mixed size can broaden the absorption band. A genetic optimization algorithm is adopted to design the anechoic layer with scatterers of mixed size at a desired frequency band from 2 kHz to 10 kHz for normal incidence, and the influence of the incident angle is also discussed.

Keywords: acoustic anechoic layer, resonant scattering, resonant absorption, singly periodic, mixed size

PACS: 43.20.+g, 43.30.Ky **DOI:** 10.1088/1674-1056/23/10/104304

1. Introduction

Acoustic anechoic layers that are attached to underwater structures are often used to reduce reflections of sound energy. To achieve good sound absorption performance, on one hand, the characteristic impedance of the layer material should be close to that of the water. Ideally, if they are equal to each other, when sound wave is incident upon the surface of the layer, no reflection will occur. On the other hand, when the sound energy goes into the layer, it is desirable to let the sound energy dissipate as much as possible to prevent further reflections at other boundaries and eventually going back to water. For impedance matching, rubber materials, whose characteristic impedance is close to water, are often used to fabricate underwater anechoic layers. However, its compressional-wave absorption is not as efficient as its shear-wave absorption. Hence, rubber layers are usually embedded with scatterers to induce scattering and wave mode conversion which can enhance the sound energy absorption. Cavity-type scatterers were used already in the Second World War,[1] and have received much attention over the past several decades.[2–13] Recently, locally resonant scatterers,[14] which consist of a soft coating layer and a heavy core, have been introduced into the design of anechoic layers and shown efficient low-frequency absorption.[15–20]

Traditionally, the scatterers in the anechoic layers are arranged in a doubly periodic lattice, however, the anechoic layers with singly periodic lattice have seldom been discussed. Recently, the rubber layer with a singly periodic array of infinite cylindrical cavities is investigated using layer-multiple scattering method.[6] It has been shown that such anechoic layers with several millimeters in thickness can provide significant reflection reduction over the frequency band between 8 kHz and 20 kHz. The author concludes that the anechoic layer with a singly periodic array of infinite cylindrical cavities can be much thinner than the anechoic layer with a doubly periodic array of spherical cavities for achieving efficient reflection reduction in the desired frequency range, under steel half space backing condition.

Besides the layer-multiple scattering method, a combined plane wave expansion (PWE) and finite element (FE) method can also be used to analyze the acoustic scattering of a singly periodic structure,[21] however, only the in-plane propagation problems were investigated, the out-of-plane propagation is rarely considered.

In the present paper, anechoic characteristics of the viscoelastic layers embedded with singly periodic cavities and locally resonant scatterers are investigated by the combined PWE and FE methods. For practical consideration, the backing condition is assumed to be a steel plate followed by air half space (steel plate-backing). For the case of oblique sound incidence, the FEM is extended to the case of out-of-plane prop-

*Project supported by the National Natural Science Foundation of China (Grant Nos. 1100429 and 51275519).

†Corresponding author. E-mail: wenxs@vip.sina.com

© 2014 Chinese Physical Society and IOP Publishing Ltd

agation. The absorption mechanism is investigated by analyzing the scattering and absorption characteristics of the scatterers. A genetic optimization algorithm is adopted to design the anechoic layer with scatterers of mixed size at a desired frequency band from 2 kHz to 10 kHz for normal incidence. Finally, spacial oblique incidence of acoustic waves is also discussed.

2. Model and method

2.1. Model: three-dimensional acoustic scattering of singly periodic anechoic layer

Figure 1 shows the model of the anechoic layer under a steel plate-backing. The viscoelastic polymer slab contains a line lattice of infinite long cylindrical scatterers. The periodic distance of the scatterer line, i.e., the lattice constant is denoted as a. The backing consists of a steel plate followed by half-infinite air space. The whole structure can be regarded as a sequence of different layers perpendicular to the y axis. The geometry of the structure is characterized by the continuous translational symmetry in the z direction, and the discrete translational symmetry with period a in the x direction. A plane compressional harmonic wave is incident from the water half space in front of the anechoic layer. For brevity, the common time factor $e^{-j\omega t}$ is suppressed. The expression of the incident wave with angular frequency ω is

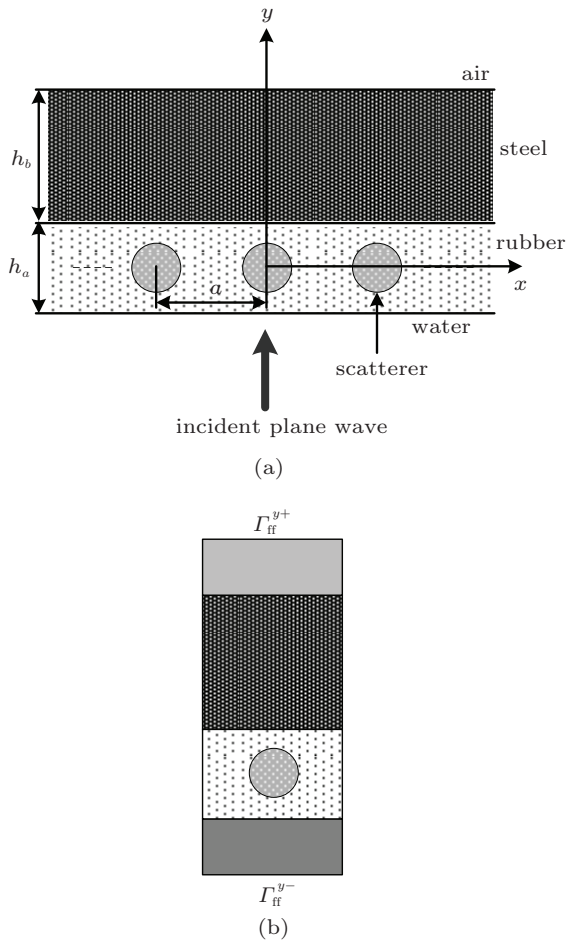


Fig. 1. (a) The structure includes a viscoelastic layer and a steel plate-backing. (b) An unit cell of the singly periodic structure.

$$p_{\mathrm{i}}(x,y,z) = p_0 \exp[\mathrm{j}(k_x x + k_y y + k_z z)], \tag{1}$$

where, $k_x = k\sin\theta\cos\varphi$, $k_y = k\sin\theta\sin\varphi$, $k_z = k\cos\theta$ is the wave number in the x, y, z directions respectively; θ and φ are the polar angle and the azimuthal angle of the incident wave vector; the total wave number of the incident wave k is given by $k = \omega/c$, where c is the sound speed of water. The incident sound is scattered by the structure. The scattered sound contains the reflection to water and the transmission to air. The goal is to design the anechoic layer to minimize the reflections. Calculation for the scattered sound is the first step which will be discussed in this section.

2.2. Combined plane wave expansion and finite element method

The in-plane propagation problem, i.e., the case of $k_z = 0$, ($\theta = 0$), has been discussed in Ref. [21] by using a combined plane wave expansion and finite element method. In the following, it will be extended to solve the out-of-plane propagation problem, i.e., the case of $k_z \neq 0$, ($\theta \neq 0$).

The key point to make this extension is utilizing the continuous translational symmetry of the structure in the z direction. According to the wave propagation theory, the components of the wave vector along the continuous translational symmetry directions are conserved qualities. This means that the physical fields F such as displacement $\boldsymbol{u}$, stress $\boldsymbol{\sigma}$ in the solid, acoustic pressure p in the fluid, etc. can be written as

$$F(x,y,z) = F(x,y)\exp(\mathrm{j}k_z z). \tag{2}$$

Because the z-dependent component of the physical fields is known as $\exp(\mathrm{j}k_z z)$, the unknown (x,y)-dependent component $F(x,y)$ needs to be calculated. Hence, the original three-dimensional problem which is (x,y,z)-dependent can be reduced to a two-dimensional problem, i.e., (x,y)-dependent.

According to the well-known three-dimensional (x,y,z)-dependent wave equations of acoustic medium and solid medium, we can drive the governing equations for the (x,y)-dependent physical fields by using the relation (2),

$$\begin{aligned} &\nabla^2 p(x,y) + k_{f,xy}^2 p(x,y) = 0, \\ &\widetilde{\nabla}\cdot\boldsymbol{\sigma}(x,y) + \omega^2\rho\boldsymbol{u}(x,y) = \boldsymbol{0}, \end{aligned} \tag{3}$$

where $\nabla = [\partial/\partial x, \partial/\partial y]^{\mathrm{T}}$, $\widetilde{\nabla} = [\partial/\partial x, \partial/\partial y, \mathrm{j}k_z]^{\mathrm{T}}$. The $k_{f,xy}$ is the component of the acoustic wave vector along the x–y plane, and equal k_{xy} for water, k'_{xy} for air. $\boldsymbol{\sigma}(x,y)$ is the (x,y)-dependent component of the stress in solid. It is a function of

displacements $\boldsymbol{u}(x,y)$,

$$\boldsymbol{\sigma}(x,y)=\lambda(\widetilde{\nabla}\cdot\boldsymbol{u}(x,y))\boldsymbol{I}+\mu\left[\widetilde{\nabla}\boldsymbol{u}(x,y)+(\widetilde{\nabla}\boldsymbol{u}(x,y))^{\mathrm{T}}\right], \quad (4)$$

where λ, μ represent the Laméelastic constants. The compressional and shear wave speeds c_ℓ and c_t are related to the Laméconstants via

$$c_\ell=\sqrt{\frac{\lambda+2\mu}{\rho_{\mathrm{s}}}},\quad c_t=\sqrt{\frac{\mu}{\rho_{\mathrm{s}}}}, \quad (5)$$

The principle of virtual work for the acoustic medium and solid medium yields the variational equations for the domain of the unit cell of the structure as shown in Fig. 1(b),

$$\begin{aligned}&\int_{\Omega_{\mathrm{f}}}\Big\{\delta p(x,y)\big[-\omega^2(1/c_{\mathrm{f}}^2-\cos^2\theta/c^2)p(x,y)\big]\\&+\nabla\delta p(x,y)\cdot\nabla p(x,y)\Big\}\mathrm{d}\Omega\\&+\int_{\Gamma_{\mathrm{sf}}}\{\delta p(x,y)\nabla p(x,y)\cdot\boldsymbol{n}_{\mathrm{s},xy}\}\mathrm{d}\Gamma\\&=\int_{\Gamma_{\mathrm{ff}}}\{\delta p(x,y)\nabla p(x,y)\cdot\boldsymbol{n}_{xy}\}\mathrm{d}\Gamma,\end{aligned} \quad (6)$$

and

$$\begin{aligned}&\int_{\Omega_{\mathrm{s}}}\Big\{\delta\boldsymbol{u}(x,y)\cdot[-\omega^2\rho_{\mathrm{s}}\boldsymbol{u}(x,y)]\\&+[\widetilde{\widetilde{\nabla}}\delta\boldsymbol{u}(x,y)]:\boldsymbol{\sigma}(x,y)\Big\}\mathrm{d}\Omega\\&-\int_{\Gamma_{\mathrm{sf}}}\{\delta\boldsymbol{u}(x,y)\cdot(\boldsymbol{\sigma}\cdot\boldsymbol{n}_{\mathrm{s}})\}\mathrm{d}\Gamma\\&=\int_{\Gamma_{\mathrm{ss}}}\{\delta\boldsymbol{u}(x,y)\cdot(\boldsymbol{\sigma}(x,y)\cdot\boldsymbol{n})\}\mathrm{d}\Gamma,\end{aligned} \quad (7)$$

where $\delta p(x,y)$ and $\delta\boldsymbol{u}(x,y)$ represent admissible variations of the unknown acoustic pressure and of the unknown displacement vector, respectively. c_{f} is the sound speed of the acoustic medium, $c_{\mathrm{f}}=c$ for water domain, $c_{\mathrm{f}}=c'$ for air domain. Ω_{f} and Ω_{s} are the fluid domain and the solid domain, Γ_{sf} is the solid–fluid interface, Γ_{ff} is the fluid–fluid interface which contains the periodic boundary of the fluid part and the boundaries $\Gamma_{\mathrm{ff}}^{y-}$ and $\Gamma_{\mathrm{ff}}^{y+}$ (see Fig. 1(b)), and Γ_{ss} is the solid–solid interface which contains the periodic boundaries of the solid part. $\boldsymbol{n}$ represents the out normal unit vector of the boundary. $\boldsymbol{n}_s$ represents the normal unit vector of the acoustic–solid interaction boundary with direction from solid towards fluid. $\boldsymbol{n}_{xy}$ and $\boldsymbol{n}_{\mathrm{s},xy}$ are two-dimensional vectors. $\boldsymbol{n}_{xy}$ is composed of the x- and y-components of the spacial vector $\boldsymbol{n}$, and $\boldsymbol{n}_{\mathrm{s},xy}$ of spacial vector $\boldsymbol{n}_{\mathrm{s}}$. The spatial differential operator $\widetilde{\widetilde{\nabla}}$ is defined as $\widetilde{\widetilde{\nabla}}=[\partial/\partial x,\partial/\partial y,-\mathrm{j}k_z]^{\mathrm{T}}$.

The continuity of the normal component of the particle displacement and the stress at the acoustic–solid interaction boundary leads to

$$\begin{aligned}&\frac{1}{\rho_{\mathrm{f}}}\nabla p(x,y)\cdot\boldsymbol{n}_{\mathrm{s},xy}=\omega^2\boldsymbol{u}(x,y)\cdot\boldsymbol{n}_{\mathrm{s},xy},\\&\boldsymbol{\sigma}(x,y)\cdot\boldsymbol{n}_{\mathrm{s}}=-p(x,y)\boldsymbol{n}_{\mathrm{s}},\end{aligned}\quad (x,y)\in\Gamma_{\mathrm{sf}}. \quad (8)$$

Substituting Eq. (8) to the variational Eqs. (6) and (7), a linear system can be induced by the standard finite element discretization approximation procedure.[22]

The process for dimension reduction is done, but the vector on the right of the linear system contains unknown components corresponding to the physical fields at the periodic boundaries and the boundaries $\Gamma_{\mathrm{ff}}^{y-}$ and $\Gamma_{\mathrm{ff}}^{y+}$. The procedure for eliminating these unknown components can follow the approach presented in Ref. [21]. The idea is to utilize the discrete translational symmetry of the structure in the x direction. According to Bloch theorem in wave propagation theory, the discrete translational symmetry with period a in the x direction implies the physical fields $F(x,y)$ satisfying the Bloch condition

$$F(x+a,y)=\exp(\mathrm{j}k_xa)F(x,y), \quad (9)$$

and the reflected sound $p_{\mathrm{r}}(x,y)$ and transmitted sound $p_{\mathrm{t}}(x,y)$ can be expanded as the summation of plane waves in a discrete wave vector space,

$$\begin{aligned}p_{\mathrm{r}}(x,y)&=\sum_{m=-\infty}^{\infty}R_m\exp[\mathrm{j}(k_{xm}x-k_{ym}y)],\\p_{\mathrm{t}}(x,y)&=\sum_{m=-\infty}^{\infty}T_m\exp[\mathrm{j}(k_{xm}x+k'_{ym}y)],\end{aligned} \quad (10)$$

in the above expressions, $k_{xm}=k_x+2\pi m/a$, $k_{ym}=\sqrt{k_{xy}^2-k_{xm}^2}$, $k'_{ym}=\sqrt{k'^2_{xy}-k_{xm}^2}$; and $k_{xy}=\sqrt{k^2-k_z^2}$, $k'_{xy}=\sqrt{k'^2-k_z^2}$, $k'=\omega/c'$, c' is the sound speed of air. For computational consideration, one has to truncate the Fourier series in Eq. (10) using a number of spatial harmonics large enough to ensure convergence. The equations (9) and (10) are the key points for calculating $F(x,y)$ in the unit cell. Assuming $2M+1$ terms in plane wave expansions (10), the plane wave expansion coefficients $\{R_m\}_{m=-M}^{M}$ and $\{T_m\}_{m=-M}^{M}$ can be calculated by matching acoustic fields at two boundaries $\Gamma_{\mathrm{ff}}^{y-}$ and $\Gamma_{\mathrm{ff}}^{y+}$ (see Fig. 1(b)), when the acoustic field $p(x,y)$ is solved.

The anechoic performance of the structure is characterized by the reflection coefficients $\mathscr{R}$ which is defined by the ratio of the reflected energy per unit area of the structure per unit time to the incident energy per unit area of the structure per unit time.[23] The time average power flux of the sound is given by $\boldsymbol{P}=\mathrm{Re}\{p\boldsymbol{v}^*\}/2$. The incident energy per unit area of the structure per unit time is given by the magnitude of the y component of $\boldsymbol{P}_{\mathrm{in}}$, and the reflected energy per unit area of the structure per unit time is given by the magnitude of the y

component of $\boldsymbol{P}_{\rm rf}$. By definition the reflection coefficient is given by

$$\mathscr{R} = \frac{\sum_{m=-M'}^{M'} |R_m|^2 k_{ym}}{|p_0|^2 k_y}, \tag{11}$$

where M' represents the largest rank of the propagating plane wave component of the reflected wave. Similarly, the transmission coefficient $\mathscr{T}$ is defined by the transmitted energy per unit area of the structure per unit time to the incident energy per unit area of the structure per unit time, and given by

$$\mathscr{T} = \frac{\rho \sum_{m=-M''}^{M''} |T_m|^2 k'_{ym}}{\rho' |p_0|^2 k_y}, \tag{12}$$

where M'' represents the largest rank of the propagating plane wave component of the transmitted wave. The absorption coefficient of the structure is

$$\mathscr{A} = 1 - \mathscr{R} - \mathscr{T} \tag{13}$$

because of the energy conservation.

3. Anechoic characteristics and mechanisms

The analysis method proposed in Section 2 can be used for analyzing the echo reduction performance of the anechoic layer. An important advantage is the flexibility to model different types of structures. Anechoic characteristics of singly periodic anechoic layers with scatterers of the cavity-type and the locally resonant type will be discussed. The cross sections of the two types of scatterers are shown in Fig. 2. The anechoic mechanisms will be analyzed by revealing the connection between the absorption of the structure and the scattering/absorption behavior of the scatterers.

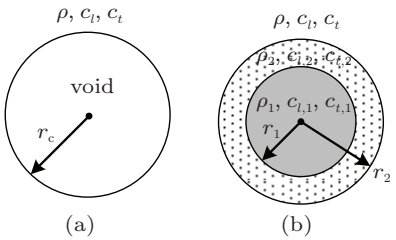


Fig. 2. (a) Void cavity, (b) locally resonant scatterer.

3.1. Anechoic characteristics

In this section, the thickness of the steel plate and the anechoic layer are 30 mm and 10 mm respectively. The wave speeds and the loss factors of the materials are assumed to be constant in the analyzed frequency range, although they should vary with frequency. The physical parameters of materials used here are listed in Table 1. η_ℓ and η_t represent the loss factors of the longitudinal module and the shear module respectively.

Table 1. Physical parameters of materials used in this section.[4,6]

Material	$\rho/(\mathrm{kg/m^3})$	$c_\ell/(\mathrm{m/s})$	$c_t/(\mathrm{m/s})$	η_ℓ	η_t
Steel	7890	5780	3220		
Rubber	1000	1500	100	0.09	0.9
Silicon rubber	1300	80	10	0.03	0.3
Water	1000	1500			
Air	1.29	340			

Setting the lattice constant to be 100 mm, figure 3(a) shows the frequency variation of the reflection ($10\log\mathscr{R}$) of the anechoic layers with cavities of different sizes. They all provide one reflection trough in the considered frequency range. It is observed that the reflection trough moves to lower frequency while increasing the cavity size, meanwhile the amplitude of the trough increases gradually.

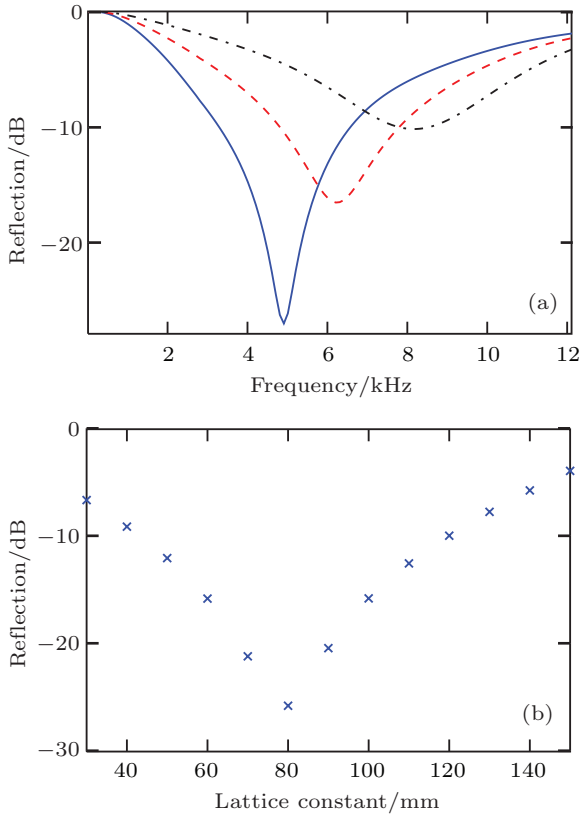


Fig. 3. (color online) (a) The reflection varied with frequency at normal incidence. The solid line, the dashed line, and the dot–dashed line are reflection curves with cavity size of 2.5 mm, 2 mm, and 1.5 mm, respectively. (b) The reflection varied with the lattice constant at the frequency 6200 Hz, with the cavity size $r_{\rm c} = 2$ mm.

The frequency of the reflection trough of the anechoic layer with cavity of $r_{\rm c} = 2$ mm is 6200 Hz. Keeping $r_{\rm c} = 2$ mm unchanged, figure 3(b) shows the variation of the reflection with the lattice constant at a chosen frequency 6200 Hz which corresponds to the above reflection trough. It is observed that the reflection decreases with the lattice constant decreasing from 150 mm to 80 mm, and increases with the lattice constant from 80 mm to 30 mm.

Figure 4(a) shows the variation of the reflection of the anechoic layers with locally resonant scatterers of different

sizes. In the present computation, the lattice constant is 50 mm. There exist two significant reflection troughs in the considered frequency range. The frequency and the amplitude of the reflection troughs increase with the scatterer size decreasing. For analyzing the influence caused by the lattice constant, we set the scattering size to be 4 mm, let the lattice constant vary from 150 mm to 30 mm. The frequencies of the two reflection troughs of the anechoic layer with locally resonant scatterers of $r_2 = 4$ mm are 1700 Hz and 5000 Hz. Figure 4(b) shows the reflection curves variation with the lattice constant at frequencies of 1700 Hz and 5000 Hz respectively. It is observed that the reflection decreases when the lattice constant decreases for the case of the frequency equaling 1700 Hz. For the case of the frequency equaling 5000 Hz, the reflection decreases with the lattice constant decrease from 150 mm to 110 mm, but increases with the lattice constant decrease from 110 mm to 30 mm.

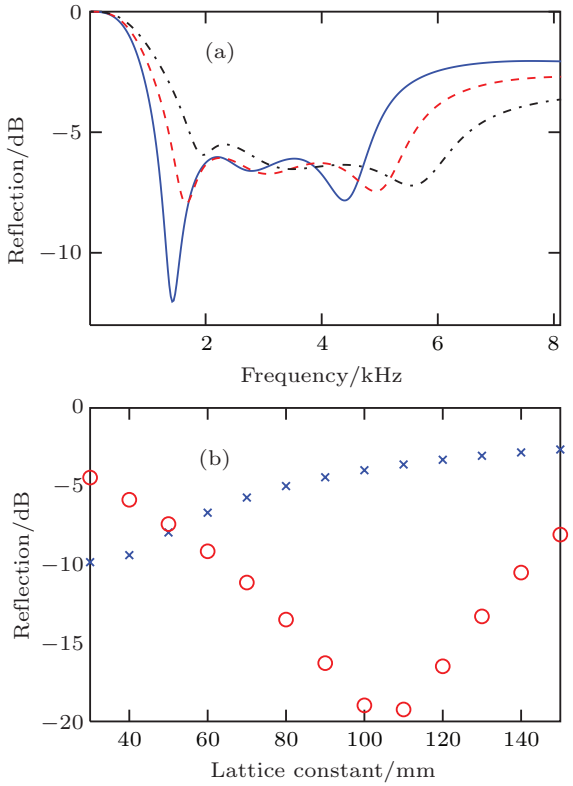


Fig. 4. (color online) (a) The reflection varied with frequency at normal incidence. The solid line, the dashed line, and the dot–dashed line are reflection curves with scatterer size r_2 of 4.5 mm, 4 mm, and 3.5 mm respectively. The ratio r_1/r_2 is fixed as 0.6. (b) The reflection varied with the lattice constant, with the scatterer size $r_2 = 4$ mm. The cross markers and the circle markers are reflection curves for the frequency of 1700 Hz and 5000 Hz respectively.

3.2. Absorption mechanisms

Due to the medium of the transmitted space is air, the impedance of which is mismatched with steel critically, the transmission $\mathscr{T}$ is almost zero. Hence, the relation $\mathscr{A} \approx 1 - \mathscr{R}$ is satisfied. The more the sound energy absorbed, the less the sound energy reflected. The normal incident sound excites compressional wave in rubber. The excited compressional wave energy is scattered by the scatterers and the backing. If the scatterers contain viscoelastic materials, the wave energy can be absorbed by the scatterers. The rubber materials absorb part of the scattered energy, the remainder of which goes back into water and composes the reflection. The reflection or the absorption characteristics of the anechoic layers should relate to the scattering and absorption behavior of the single scatterer which can be characterized by the scattering cross section and the absorption cross section respectively.

The scattering cross section of a scatterer is defined as the ratio of the time-averaged power flux scattered in all directions by the scatter to the intensity of the incident plane wave $I_{\rm i}$,[24]

$$\sigma_{\rm sc} = P_{\rm sc}^{\infty}/I_{\rm i} = \lim_{r\to\infty} \frac{1}{I_{\rm i}} \int_{S_{\rm r}} {\rm Im}\left\{\frac{1}{2}\omega \boldsymbol{u}_{\rm sc}^{*} \cdot \boldsymbol{\sigma}_{\rm sc}\right\} \cdot \hat{\boldsymbol{n}} \,{\rm d}S. \quad (14)$$

In the case where the scatterer is infinitely long cylindrical, $S_{\rm r}$ represents the cylindrical surface of r-radius and one-meter length. The absorption cross section is the ratio of the time-averaged power transferred into the region with unit-length surface $S_{\rm r}$ that contains the scatterer to the intensity of the incident plane wave,[24]

$$\sigma_{\rm ab} = \frac{1}{I_{\rm i}} \int_{S_{\rm r}} -{\rm Im}\left\{\frac{1}{2}\omega \boldsymbol{u}^{*} \cdot \boldsymbol{\sigma}\right\} \cdot \hat{\boldsymbol{n}} \,{\rm d}S. \quad (15)$$

The scattering cross section and the absorption cross section have analytical expressions which can be deduced by cylindrical wave expansion method. Assuming that the incident wave is compressional,

$$\boldsymbol{u}_{\rm in} = u_{\rm in} \exp({\rm j}\boldsymbol{K} \cdot \boldsymbol{r}) \hat{\boldsymbol{e}}(\boldsymbol{K}). \quad (16)$$

The incident plane wave and the scattered wave can be written as[25–27]

$$\begin{aligned} \boldsymbol{u}_{\rm in}(r,\theta) &= \sum_{n\sigma} a_{n\sigma} \boldsymbol{j}_{n\sigma}(r,\theta), \\ \boldsymbol{u}_{\rm sc}(r,\theta) &= \sum_{n\sigma} b_{n\sigma} \boldsymbol{h}_{n\sigma}(r,\theta), \end{aligned} \quad (17)$$

where $\boldsymbol{j}_{n\sigma}(r,\theta)$ and $\boldsymbol{h}_{n\sigma}(r,\theta)$ are vector cylindrical wave functions. The scattered wave coefficients $b_{n\sigma}$ can be solved by T-matrix method.[25] Using the orthonormal relation and the asymptotic expressions of the cylindrical wave functions, we can get the following simple expressions for the scattering cross section and the absorption cross section,

$$\sigma_{\rm sc} = \frac{4\alpha}{|u_{\rm in}|^2} \sum_{n\sigma} |b_{n\sigma}|^2, \quad (18)$$

$$\sigma_{\rm ab} = -\frac{4\alpha}{|u_{\rm in}|^2} \sum_{n} \left\{{\rm Re}\{a_{nL}^{*} b_{nL}\} + |b_{nL}|^2 + |b_{nM}|^2\right\}. \quad (19)$$

Figure 5 shows the scattering cross section curves of the cavities mentioned in Subsection 3.1. It is observed that there exists one resonance peak at the frequency near the reflection trough. Hence, it is concluded that the reflection trough is caused by the resonance scattering of the cavity. The scattered wave is dissipated by the rubber materials, then the reflection is reduced significantly.

Moreover, the intensity of the total scattered wave by the lattice of cavities is not only related to the cavity size, but also related to the lattice constant due to the multiple scattering effect between the cavities. The multiple scattering effect can be strengthened by reducing the lattice constant. Figure 3(b) shows that, when the lattice constant is large enough (between 80 mm–150 mm), the wave energy scattered by the cavity lattice can be absorbed efficiently. As a result, the reflection decreases with the decrease of the lattice constant. When the lattice constant is not large enough (between 30 mm–80 mm), the total scattered wave cannot be absorbed efficiently, and therefore the reflection increases with the decrease of lattice constant.

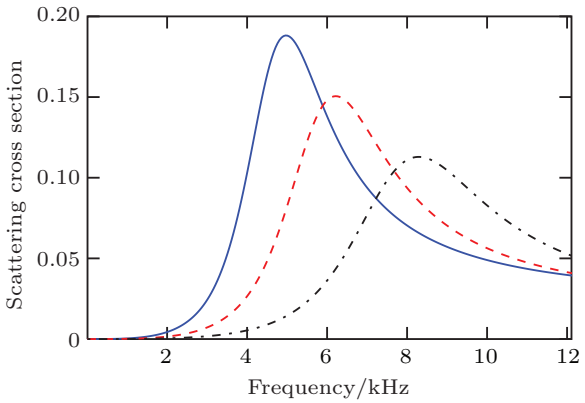


Fig. 5. (color online) The scattering cross sections of the cavity, the solid line, the dashed line, and the dot–dashed line correspond to the cavity sizes 2.5 mm, 2 mm, and 1.5 mm, respectively.

Figure 6(a) shows the scattering cross sections of the locally resonant scatterers mentioned in Subsection 3.1, and figure 6(b) shows the corresponding absorption cross sections. It is observed that there exists one peak in the scattering cross sections curve, and the peak frequency is close to the second reflection trough in Fig. 4(a). As shown in Fig. 6(b), there exist two peaks in the absorption cross sections curve, and the frequencies of the two peaks are close to the two reflection troughs in Fig. 4(a) respectively. One can conclude that the first reflection trough of the structure is mainly caused by the resonant absorption of the locally resonant scatterers. The steel core exhibits a rigid body resonance as shown in Fig. 7(a). The motion of the core forces the coating to vibrating accordingly, then the wave energy is dissipated in the coating. The second reflection trough of the structure is caused by the resonant scattering and absorption of the locally resonant scatterers. The steel core presents much less vibration than that of the coating, the coating presents resonant vibrating, as shown in Fig. 7(b). The incident wave is dissipated in the coating and scattered back into the rubber matrix. For the first resonant mode, the wave energy is mainly trapped and absorbed in the scatterers, the multiple scattering among the scatterers is weak. Hence, the reflection decreases with the lattice constant decreasing at the first resonance frequency, which is shown as the cross mark curve in Fig. 4(b). Because the second resonant mode presents resonant scattering, the multiple scattering among the scatterers is enhanced. The reflection of the locally resonant structure with the variation of lattice constant (the circle mark curve in Fig. 4(b)) follows a similar pattern as that of the cavity-type anechoic structure (Fig. 3(b)).

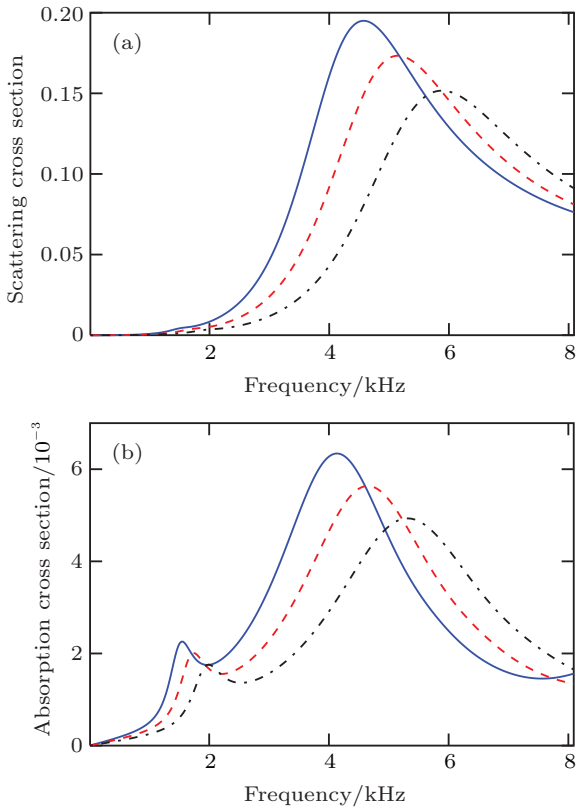


Fig. 6. (color online) (a) The scattering cross sections of the locally resonant scatterers; (b) the absorption cross sections of the locally resonant scatterers. The solid line, the dashed line, and the dot–dashed line correspond to scatterer sizes 4.5 mm, 4 mm, and 3.5 mm respectively.

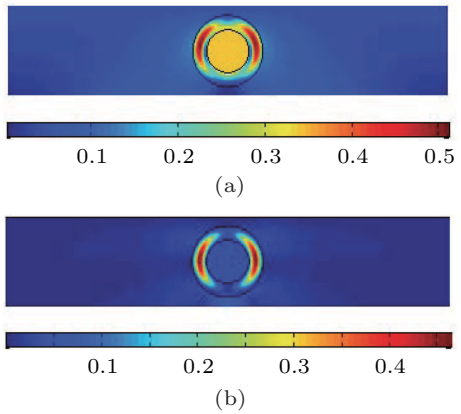


Fig. 7. (color online) The displacement amplitude fields at (a) the first resonant frequency and (b) the second resonant frequency.

4. Optimal design

Efficient absorption performance can be obtained by embedding cavities or locally resonant scatterers into the rubber layer, but the bandwidth is narrow. The efficient absorption

is related to the resonance behavior of the scatterers, and the resonance frequencies are varied with the size of the scatterer. Hence, the bandwidth of efficient absorption may be broadened by using scatterers of the mixed size. The structure considered here is shown in Fig. 8. The lattice constant is a.

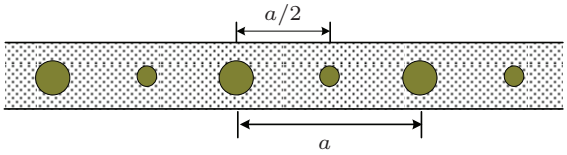


Fig. 8. (color online) The structure of the anechoic layer with a single periodic lattice of mixed size scatterers.

The genetic algorithm[28–30] is used to design anechoic layers. When considering the balance of the worst performance and the average performance through the frequency range, the objective function of the optimization problem is weighted average of the maximum and the mean value of the reflection in the design frequency range $[f_1, f_2]$ at normal incidence,

$$\Psi(\mathscr{D}) = q\left(\sup_{f\in[f_1,f_2]} \mathscr{R}(f;\mathscr{D})\right) + (1-q)\left(\frac{1}{f_2-f_1}\int_{f_1}^{f_2}\mathscr{R}(f;\mathscr{D})\,\mathrm{d}f\right), \quad (20)$$

where $\mathscr{D}$ represents the set of design variables, and the weight $q \in [0,1]$. The objective is to find the values of the design variables that can minimize the value of the objective function. In the following discussion, the weight q is set as 0.5 and the frequency range is set from 2×10^3 Hz to 1×10^4 Hz.

For optimal design of the cavity-type anechoic layers, the thickness is set as 10 mm, and the mechanical parameters of the rubber material are fixed as $\rho = 1000$ kg/m^3, $c_\ell = 1500$ m/s, $c_t = 100$ m/s, $\eta_\ell = 0.05$, $\eta_t = 0.5$. Three design variables, the radius of the larger cavities r_1, the ratio of the radius of the small cavities to the radius of the larger cavities r_2/r_1, and the lattice constant a, are allowed in the following search space: $r_1 \in [1.5,3]$ mm, $r_2/r_1 \in [0.2,\ 1]$, $a \in [20,120]$ mm. Table 2 shows the optimized values of the design variables. Figure 9(a) shows the anechoic performance of the optimized structure. It can be observed that the reflection of the optimized structure is below -7 dB, i.e., the absorption coefficients are above 0.8 in the design frequency range 2×10^3 Hz $\sim 1\times10^4$ Hz.

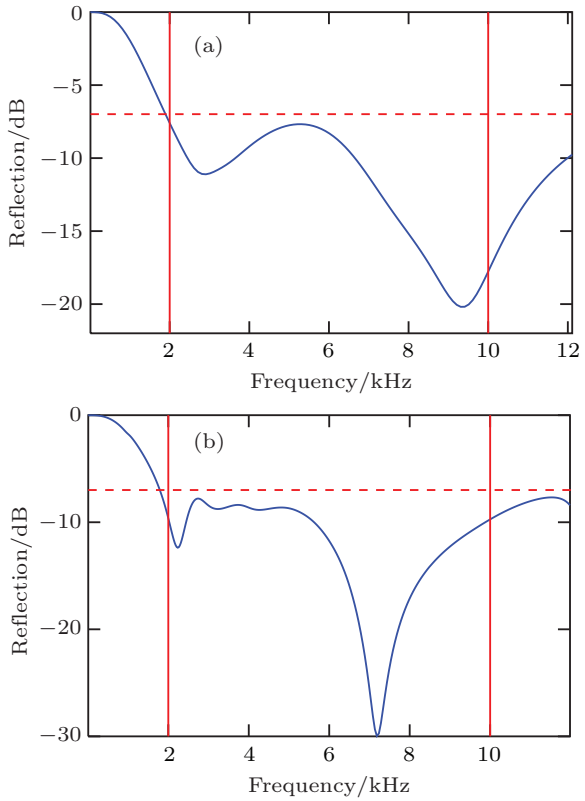


Fig. 9. (color online) (a) Reflection of the cavity-type anechoic layer obtained by genetic optimization at normal incidence; (b) Reflection of the locally resonant-type anechoic layer obtained by genetic optimization at normal incidence.

For optimal design of the locally resonance-type anechoic layers, the thickness is also set as 10 mm. For the rubber material, except that the shear wave speed is allowed within the search interval $[100,200]$ m/s, the density, the compressional wave speed, and the loss factors are fixed as $\rho = 1000$ kg/m^3, $c_\ell = 1500$ m/s, $\eta_\ell = 0.05$, $\eta_t = 0.5$. For the silicon rubber, the density and the loss factor are fixed as $\rho^{\mathrm{sr}} = 1300$ kg/m^3, $\eta_\ell^{\mathrm{sr}} = 0.03$, $\eta_t^{\mathrm{sr}} = 0.3$, and the compressional wave speed c_ℓ^{sr} and the ratio $c_t^{\mathrm{sr}}/c_\ell^{\mathrm{sr}}$ are varied with the search intervals $[25,80]$ m/s and $[0.1,0.3]$, respectively. For the locally resonant scatterers, the ratio of the radius of the core to the radius of the scatterer is fixed as 0.6, and the radius of the larger scatterer r_1 and the ratio of the radius of the small scatterer to the radius of the larger scatterer are allowed in the search intervals $[2.5,4.5]$ mm and $[0.3,1]$ respectively. The search interval of the lattice constant is set as $[30,100]$ mm. Table 3 shows the optimized values of the design variables. Figure 9(b) shows the anechoic performance of the optimized structure. It can also be observed that the reflection of the optimized structure is below -7 dB in the design frequency range of 2×10^3 Hz $\sim 1\times10^4$ Hz.

Table 2. Specification of the optimized anechoic layer for the curve of Fig. 9(a).

r_1/mm	r_2/r_1	a/mm
2.9135	0.3381	77.6439

Table 3. Specification of the optimized anechoic layer for the curve of Fig. 9(b).

a/mm	r_1/mm	r_2/r_1	c_t^{r}/(m/s)	c_ℓ^{sr}/(m/s)	$c_t^{\mathrm{sr}}/c_\ell^{\mathrm{sr}}$
92.9724	3.5663	0.4027	111.2229	34.7965	0.1353

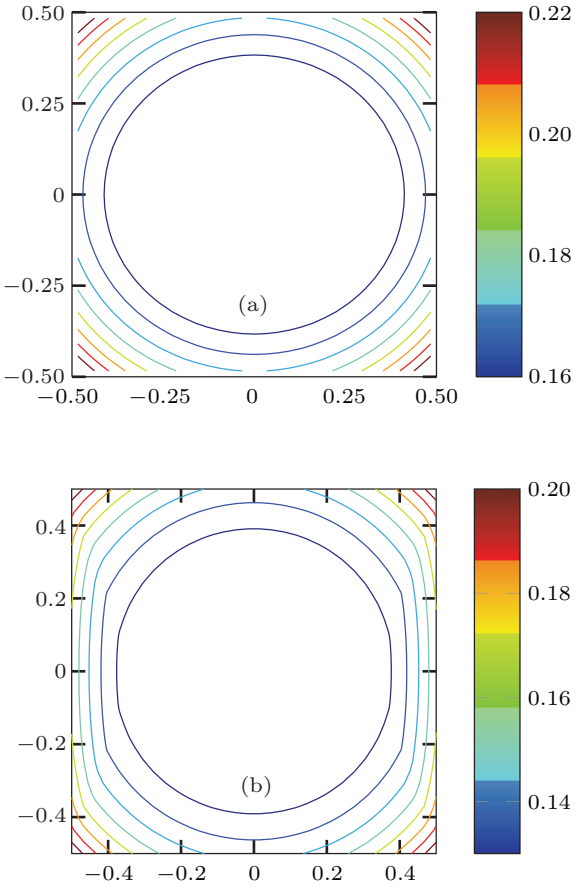


Fig. 10. (color online) Level curves for the value of the objective function as a function of direction of the incident wave. The horizontal axis and the vertical axis represent the projection of a unit vector in the direction of the incident wave to the x axis and the z axis respectively. (a) For the cavity-type anechoic layer, (b) for the locally resonant-type anechoic layer.

The optimization procedure is focused on the normal incidence. In order to check the performance with the variation of the incident angle, the value of the objective function defined in Eq. (17) at oblique incidence is computed and the level curves for the results are shown in Fig. 10. The horizontal coordinate and the vertical coordinate indicate the projection of the unit direction vector of the incident wave onto the x axis and the z axis respectively. The results show that the anechoic performance reduces with incident angle increasing, however, the reduction is not significant. It is noticed that the level curves are in approximately circular shape, which indicates that the influence of the polar part and the azimuthal part of the incident direction on the anechoic performance are very similar.

5. Conclusions

We have extended the combined PWE and FE method for out-of-plane incidence, and the reflection characteristics of the anechoic layers with a singly periodic array of cavities and locally resonant scatterers are analyzed. By analyzing the scattering and the absorption behavior of the scatterers, the absorption mechanisms of the anechoic layers are revealed. The efficient absorption of the cavity-type anechoic layer is caused by the resonant scattering of the cavities. For the locally resonant-type structure, there exist two resonant modes which induce significant sound absorption of the structure. The first mode is the rigid body resonance of the steel core, and the wave absorption takes place mainly in the coating of the scatterer. The scattered wave by the scatterers is weak. The second mode is the coating resonance, the wave absorption is induced by the resonance absorption and scattering of the scatterer. The reflection characteristics of the anechoic layer is related to the lattice constant, due to the multiple scattering among the scatterers. The patterns of the influence of the lattice constant on the resonant modes are different, and the reason is explained.

The resonant scattering of the cavities and the resonant scattering/absorption of the locally resonant scatterers can lead to efficient acoustic absorption, but the frequency band of efficient absorption is narrow. Owing to the fact that the resonant frequency is related to the size of the scatterers, we use the structure with scatterers of the mixed size to broaden the band of efficient absorption. The problem of structure design for implementation efficient absorption from 2 kHz to 10 kHz is solved by generic optimization algorithm. The optimized anechoic layer of the cavity type and that of the locally resonant type achieves efficient absorption over the design frequency range. The influence of the incident angle is also investigated. The results show that the anechoic performance of the optimized structures tends to get slightly worse as the incident angle is increased. The influence of the polar part and the azimuthal part of the incident direction on the anechoic performance are very similar.

References

[1] Oberst H 1957 *Technical Aspects of Sound* (Amsterdam: Elsevier) p. 287
[2] Zhu W Q 1981 *Acta Acoustica* **2** 114 (in Chinese)
[3] Ivansson S M 2006 *J. Acoust. Soc. Am.* **119** 3558
[4] Ivansson S M 2008 *J. Acoust. Soc. Am.* **124** 1974
[5] Ivansson S M 2009 *Advances in Acoustics and Vibration* **2009** 1
[6] Ivansson S M 2012 *J. Acoust. Soc. Am.* **131** 2622
[7] Zhao H G, Liu Y Z, Wen J H, Yu D L and Wen X S 2007 *Acta Phys. Sin.* **56** 4700 (in Chinese)
[8] Tan H B, Zhao H and Xu H T 2003 *Acta Acoustica* **28** 277 (in Chinese)
[9] Tang W L, He S P and Fan J 2005 *Acta Acoustica* **30** 289 (in Chinese)
[10] Bai G F, Liu B L, Sui F S, Liu K and Yang J 2012 *Acta Acoustica* **37** 263 (in Chinese)
[11] Gaunaurd G 1977 *J. Acoust. Soc. Am.* **62** 298
[12] Lane R 1981 *Ultrasonics* **19** 28
[13] Tao M and Hua H X 2011 *Journal of Vibration and Control* **18** 48
[14] Liu Z Y, Zhang X X, Mao Y W, Zhu Y Y, Yang Z Y, Chan C T and Sheng P 2000 *Science* **289** 1734
[15] Zhao H G, Liu Y Z, Wen J H, Yu D L, Wang G and Wen X S 2006 *Chin. Phys. Lett.* **23** 2312

[16] Zhao H G, Wen J H, Yu D L and Wen X S 2010 *J. Appl. Phys.* **107** 023519
[17] Meng H, Wen J H, Zhao H G and Wen X S 2012 *Journal of Sound and Vibration* **331** 4406
[18] Lü L M, Wen J H, Zhao H G, Meng H and Wen X S 2012 *Acta Phys. Sin.* **61** 214302 (in Chinese)
[19] Wen J H, Zhao H G, Lü L M, Yuan B, Wang G and Wen X S 2011 *J. Acoust. Soc. Am.* **130** 1201
[20] Zhao H G, Wen J H, Yang H B, Lü L M and Wen X S 2014 *Appl. Acoustics* **76** 48
[21] Hennion A C, Bossut R, Decarpigny J N and Audoly C 1990 *J. Acoust. Soc. Am.* **87** 1861
[22] Zienkiewicz O C, Taylor R L and Zhu J Z 2005 *The Finite Element Method: Its Basis and Fundamentals* (New York: Elsevier)
[23] Kinsler L E, Frey A R, Coppens A B and Sanders J V 2000 *Fundamentals of Acoustics* (New York: John Wiley & Sons)
[24] Tan T H 1976 *J. Acoust. Soc. Am.* **59** 1265
[25] Varatharajulu V and Pao Y H 1976 *J. Acoust. Soc. Am.* **60** 556
[26] Varadan V V 1978 *J. Acoust. Soc. Am.* **63** 1014
[27] Wang Y J and Zhu W Y 1996 *Chin. Phys. Lett.* **13** 20
[28] Goldberg and David E 1989 *Genetic Algorithms in Search, Optimization and Machine Learning* (Baston: Addison-Wesley)
[29] Conn A R, Gould N I M and Toint Ph L 1991 *SIAM Journal on Numerical Analysis* **28** 545
[30] Conn A R, Gould N I M and Toint Ph L 1997 *Math. Comput.* **66** 261